ARTICLE

# Crystallographic, Spectroscopic, and Computational Characterization of a Diiodonaphthoquinone Diarylethene Photochrome: Halogen Bonding and Photocrystallography

Received 00th January 20xx,
Accepted 00th January 20xx

DOI: 10.1039/x0xx00000x

Shea D. Myers,[a,†] Zoe Y. Marr, [a,†] Jade A. Sency,[b] Travis B. Mitchell,[a] Jason B. Benedict[a]* and Dinesh G. Patel[b]*

We report the synthesis and characterization of 2,3-bis(5-iodo-2-methylthiophen-3-yl)naphthalene-1,4-dione and its ring-closed isomer. The ring-closed isomer crystallizes in the space group P21 with unit cell parameters of a = 11.93119(10), b = 7.4644(6), c = 12.4586(10), β = 117.024(2)°. Photoisomerization in solution is reversible and similar to that of other quinone based diarylethenes. The crystal structure of the ring-closed isomer consists of halogen bonded 2-D sheets. Upon irradiation, single crystals of the ring-closed isomer fracture along well-defined cleavage planes parallel to the sheet layers. Subsequent X-ray diffraction measurements revealed that the light-induced fracturing is due to the formation of the ring-open isomer.

## Introduction

Photochromism is defined as the ability of a compound to photochemically switch between two isomeric states with each of these states having its own unique optical, structural, and electrochemical characteristics.[1] Among the many classes of photochromic compounds, diarylethenes (DAEs, as an example quinone containing compounds **1** and **2**, Scheme 1) have gained attention owing to their fatigue resistance[2-4] and potential for use as data storage media[5, 6], sensors,[7, 8] and probes[9] including dosimeters.[10] Additionally, they have been used in biological applications[11, 12] and even for catalyst control. [13, 14]

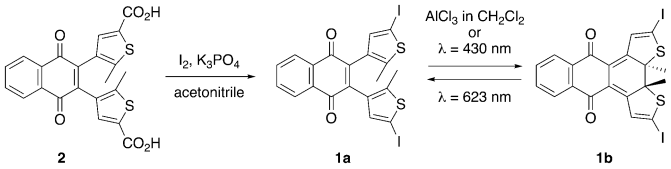


**Scheme 1.** The synthesis and photochromic response of DAE compound **1**. The chemical synthesis of closed-form **1b** from open-form **1a** is also presented.

As newer and more complex applications are envisioned, the desire to find alternatives to the high energy UV light typically required for the photoisomerization reactions has come forward as a major concern with some groups focusing on modifying the aryl portion of diarylethene photochromes.[15-17] It has been demonstrated that the use of either a quinone or naphthoquinone ethene bridge allows for visible light to initiate photoisomerization in both the ring-opening and ring-closing directions.[18-20] Quinone based headgroups are also electrochemically active[21, 22] and found in important biological molecules,[23, 24] thus making them excellent candidates for potential therapeutic agents.[25]

The rational design of DAE-based crystalline materials remains challenging and is due in part to the conformational flexibility associated with the free rotation of the aryl groups responsible for the photoactivity.[26-28] This, combined with the fact that many reported DAEs lack functional groups capable of forming reasonably strong supramolecular interactions (hydrogen bonding, halogen bonding, etc) limits DAE's potential for use in crystal engineering.[2, 5, 29] The synthesis of DAE building units in the ring-closed form which contain functional groups capable of supramolecular interactions[30-33] should facilitate the production of photoactive crystalline materials and lay the foundation for the rational design of photoactive crystalline solids.

Benzoquinone and naphthoquinone based diarylethenes are attractive candidates for these materials given the long lifetimes of the ring closed isomer and the ability of these molecules to undergo acid-promoted ring-closing reactions[12, 18, 34] thus allowing for the chromatographic isolation of pure ring-closed forms in good yields. A solution of the ring-closed isomer of 2,3-bis(2,5-dimethylthiophen-3-yl)-5,6-dimethyl-1,4-benzoquinone exhibited no ring-opening isomerization when left for 14 days in the dark at room temperature[34] indicating its thermal stability. In solution photochemical, ring closure of dithienyl quinone and naphthoquinone containing DAEs is known to proceed with efficiencies less[18, 19, 34] than that of the better known and structurally related perfluorocyclopentene containing DAEs[35]. However, chemically induced ring closure can be achieved in high yield when three equivalents of $AlCl_3$ in

[a] Department of Chemistry, University at Buffalo, Buffalo NY 14228.
[b] Department of Chemistry, The Pennsylvania State University, Hazleton PA 18202.
† Both authors contributed equally to this manuscript.
* Corresponding authors: jbb6@buffalo.edu, dgp15@psu.edu
Electronic Supplementary Information (ESI) available: [Figures S1 – S5 and tables S1 and S2]. See DOI: 10.1039/x0xx00000x

methylene chloride are added to the quinone and naphthoquinone containing ring-open isomers.[18]

Given that DAEs can provide a means for optical control of material properties, they have been synthesized with both carboxylic acid[20, 36] and pyridyl[17, 37] end groups that can allow for supramolecular assemblies through hydrogen bonding and metal-ligand interactions. Another important class of interaction in directing self-assembly, halogen bonding, has risen in popularity over the past 20 years.[38-41] However, the utilization of halogen bonding in the preparation of DAE-based crystalline solids remains relatively underexplored compared to materials based upon hydrogen bonding[36, 42, 43] or metal-ligand interactions.[44-48] Many of the properties that are unique to halogen bonding, such as tunability and variable size of the donor atom,[38] may offer specific advantages for materials designed and synthesized using these interactions.

Herein we report the synthesis, photochemistry, and structural characterization of 2,3-bis(5-iodo-2-methylthiophen-3-yl)naphthalene-1,4-dione (**1, Scheme 1**), a naphthoquinone dithienylethene containing iodine functional groups. The ring closed isomer **1b** was produced in good yield and subsequently crystallized. Analysis of the structure revealed the presence of halogen bonding interactions between the iodine and carbonyl functional groups. Photocrystallography measurements on single crystals of the ring closed isomer revealed that photo-induced cleavage of the crystals was driven by the formation of the ring-open isomer upon irradiation with visible light.

## Materials and Methods

### Materials

All chemicals were obtained from commercial sources and used as received unless otherwise noted. Acetonitrile was distilled from calcium hydride and stored over 4 Å molecular sieves prior to use. Flash column chromatography was accomplished using silica gel purchased from Fisher Scientific (230 – 400 mesh, grade 60, catalog number S825-212). Polyester backed TLC silica plates (grade 60 with UV indicator) were obtained from EMD Millipore (catalog number 1.05735.0001).

### Synthesis of Compound 1

In a 75 mL glass pressure vessel was combined iodine (2.315 g, 9.12 mmol), previously reported compound **2** (0.500 g, 1.14 mmol),[20] and anhydrous $K_3PO_4$ (0.487 g, 2.29 mmol). Anhydrous acetonitrile (10 mL) was then added in a single portion. This reaction sequence is outlined in Scheme 1. Upon sealing the vessel, the reaction was heated to 100 °C for 24 hours. After cooling to room temperature, the resulting dark solution was diluted with methylene chloride (100 mL) and washed with aqueous sodium thiosulfate (15 wt % aqueous, 2 x 50 mL) followed by one portion of saturated, aqueous sodium bicarbonate (50 mL). The remaining organic layer was dried over magnesium sulfate, filtered, and solvent removed under reduced pressure to afford a dark orange-brown solid. The solid was adsorbed onto silica, irradiated with 430 nm light, and chromatographed on silica eluting with 100% hexanes to 10% ethyl acetate in hexanes. The purple-colored closed form **1b** eluted first followed by a yellow-orange band of open form **1a**. The pure fractions of closed form were allowed to slowly evaporate yielding X-ray quality, dark purple crystals. The open form fractions were combined and solvent removed to give a dark solid (0.680 g, 99%). Spectral characterization matched that previously reported in the literature.[18]

### Preparation of 1b

In a 20 mL glass vial was placed compound **1** (0.100 g, 0.17 mmol), methylene chloride (10 mL), and $AlCl_3$ (0.066 g, granular) as depicted in Scheme 1. The dark solution was capped and stirred, turning from brown to dark green over approximately 1 – 2 minutes, for 1 hour and then diluted with water (20 mL). The organic phase was collected, washed with brine, and the crude product quickly adsorbed onto silica followed by chromatography on silica eluting with 10% ethyl acetate in hexanes. The first eluted compound was collected affording a dark purple/black solid upon removal of solvent (0.043 g, 43%). X-ray quality crystals can be obtained by slow evaporation of the chromatographic fractions.

### Spectroscopic Characterization

Solution UV-Vis spectra were obtained using a Shimadzu UV-1800 spectrometer using a home-built light source[20] for irradiation experiments. Quartz cuvettes (1 cm pathlength) were used for all solution absorption measurements. The UV-Vis spectrum of solid **1b** was obtained by gently grinding approximately 20 single crystals between two quartz plates (Starna Type 20C) to produce a microcrystalline film (thickness 5.5 μm). The plates were mounted in a cell holder (Starna CH-2049) and placed in multi-port cuvette holder (Thorlabs, CVH100) with fiber optics. The UV-Vis spectrum was obtained using a broadband UV-Vis light source (OceanInsight, DH-2000-BAL) and spectrometer (OceanInsight, HR4Pro). $^1$H-NMR characterization was performed on a Varian Inova 400 with a broadband probe operating at 400 MHz and all spectra are referenced to the residual chloroform-*d* solvent peak at 7.26 ppm.

### Computational Details

All density functional theory (DFT) calculations were performed using the computational software suite Gaussian 09 Rev. D.01 with the def2-SVP basis set.[49] The M06-2x functional was selected due to its ability to accurately model noncovalent halogen bonding interactions.[50] Gas phase geometry optimizations were performed on **1a**, **1b**, and a halogen bonded dimer consisting of two molecules of **1b**. Vibrational frequency calculations were performed for each optimized geometry to ensure the energetic minimum was obtained.

Time-dependent DFT (TD-DFT) was used to simulate the theoretical UV-vis spectra for both the open and closed-ring isomer. Twenty of the lowest energy excited states were computed for each geometry. The spectra were then generated

 

using a Gaussian broadening function with a half-width of 4000cm-1 for each transition.

**X-Ray Diffraction**

A single crystal of **1b** suitable for X-ray diffraction was mounted on the tip of a glass fiber with oil and placed on a Bruker SMART APEX II CCD diffractometer installed with a rotating anode source (Mo-Kα radiation, λ = 0.71073 Å) with a detector distance of 40.00 mm from the crystal and a 2θ-angle of -30°. During the data collection, the crystal was cooled to 90(1) K using an Oxford cryostream nitrogen gas-flow apparatus. A total of 1800 frames were collected using five 180° ω-scans (0.5° scan width) at different ϕ-angles (ϕ = 0° to 288° in 72° increments), nominally covering complete reciprocal space.

Following irradiation with broadband white light from an inverted microscope (Olympus IMT-2), a fragment of a photoirradiated slice of **1b** suitable for X-ray diffraction was mounted on the tip of a glass fiber with oil and placed on a Bruker SMART APEX II CCD diffractometer installed at a rotating anode source (Mo-Kα radiation, λ = 0.71073 Å) with a detector distance of 40.00 mm from the crystal and a 2θ-angle of -20°. During the data collection, the crystal was cooled to 90(1) K using an Oxford cryostream nitrogen gas-flow apparatus. A total of 1550 frames (25 second exposure) were collected using five 155° ω-scans (0.5° scan width) at different ϕ-angles (ϕ = 0° to 288° in 72° increments).

Data reduction was completed using SAINT version 8.40A, and a multi-scan absorption correction was applied using SADABS version 2016 included in the Bruker APEX3 software suite.[51] Space-group determination was performed using the XPREP utility included in the SHELXTL software package.[52] Using Olex2,[53] the structure was solved with ShelXT[54] using intrinsic phasing and refined with ShelXL[55] using least squares minimization (full-matrix least-squares on $F^2$). For the irradiated **1b**, conversion percentages in the lattice were determined from the refinement of the disordered sulfur atoms which arise from the superposition of the ring open and ring closed structures within the lattice. The occupancies of an open/closed pair of sulfur atoms were constrained to sum to 1.0. The resulting occupancies were taken to be the conversion percentage within the lattice where 100% is a crystal consisting entirely of ring closed molecules. Numerous attempts were made to model the disordered thiophene corresponding to the ring-open isomer. For example, refinement using the thiophene fragment from the database in Olex2 combined with EADP, DFIX, and RIGU commands added over 150 restraints, 20 parameters and increased $R_1$ by approximately 0.3 relative to the model **1b-irradiated** described herein. This suggests that the geometry of the thiophene groups corresponding to the ring-open isomer may not be appropriately and reliably captured through discrete modelling of these groups.

## Results and Discussion

**Synthesis and Solution Spectroscopic Characterization of Compound 1**

Compound **1** was obtained using the procedure of Larrosa[56] starting with dicarboxylic acid DAE **2**, the synthesis of which has been previously reported.[20] Briefly, **2** is deprotonated using potassium phosphate and then iodinated using molecular iodine in acetonitrile in a one-pot reaction (Scheme 1). Critical to the reaction's success is the temperature, which must be kept at 100 °C; consequently, the reaction was run in a pressure vessel to achieve this temperature. Irradiation of **1,** which has been adsorbed onto silica, with 430 nm light allows photoisomerization of **1a** to **1b** such that separation of open form **1a** and closed form **1b** can be achieved by column chromatography eluting with 100% hexanes to 10% ethyl acetate in hexanes. Under these conditions, **1b** elutes slightly faster than **1a.** Alternatively, pure **1b** can be obtained by treatment of **1** with $AlCl_3$.

Worthy of note, compound **1** has been previously synthesized by Deng and Liebeskind[18] using a Stille coupling route; iodination was achieved at the unsubstitituted thiophene 5-position using iodic acid and iodine in a mixture of acetic acid and carbon tetrachloride. In this study, compound **1** is obtained from compound **2** (Scheme 1), which is conveniently obtained through Suzuki coupling methodology.[20]

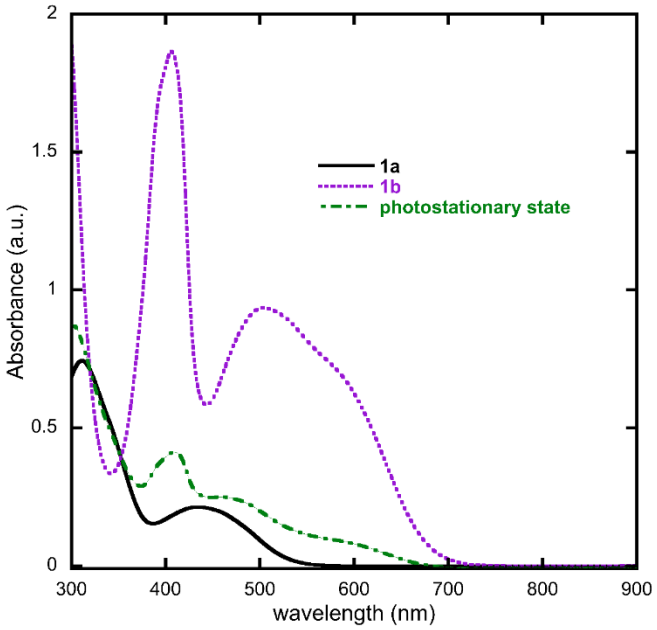


**Figure 1.** The UV-Vis spectra of **1a**, **1b**, and the photostationary state obtained after irradiation of **1a** with 430 nm light for 10 seconds. Concentrations are 9.6 x $10^{-5}$ M in methylene chloride

Compound **1a** is readily soluble in chlorinated solvents and presents a faint yellow color in dilute solutions with $\lambda_{max}$ values at 311 nm and 434 nm in methylene chloride. Treatment with aluminum chloride leads to ring closure and the formation **1b** with the appearance of new absorption bands at 406 nm and 504 nm and a shoulder near 600 nm (Figure 1 and Figure S1). There is a slight increase in intensity of the 434 nm band. Isosbestic points are observed at 319 nm and 353 nm confirming the irradiated solutions contain only two chemical species, namely the ring-open (**1a**) and ring-closed (**1b**) isomers. Figure 1 illustrates **1a**, **1b**, and the photostationary state

obtained after irradiation of **1a** with 430 nm light for 10 seconds. The time resolved spectra of the conversion is of **1a** to **1b** is presented in Figure S2. The original spectrum is regenerated upon irradiation with 623 nm light for 100 seconds (Figure S3).

### Structure and Spectroscopic Characterization of Crystalline 1b

Compound **1b** crystallizes in the monoclinic space group, $P2_1$, with a single molecule in the asymmetric unit. Crystals of **1b** grow as large (001) tablets bounded by (010), (20-1), and (22-1) as shown in Figure 2.

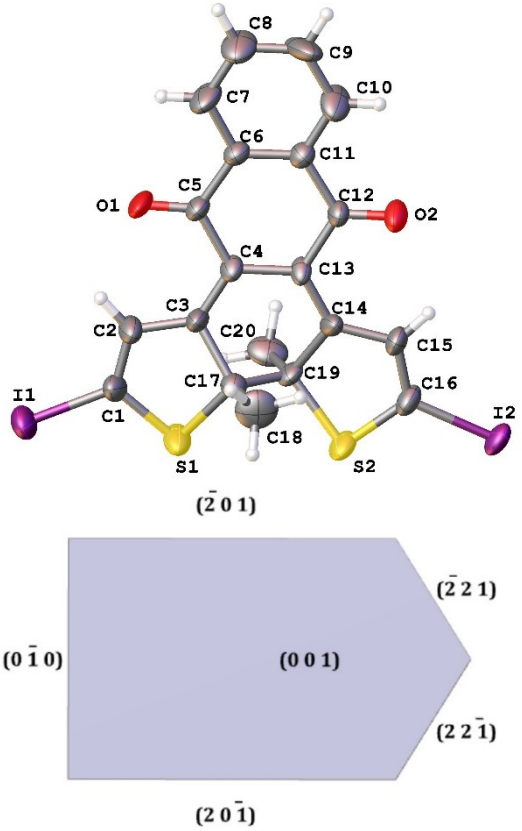


**Figure 2.** Top: The asymmetric unit of **1b** with atom labels. Bottom: Idealized habit of a single crystal of **1b** illustrating the observed crystallographic faces. [WinXmorph] Atom colors: carbon (grey), oxygen (red), hydrogen (white), sulfur (yellow), iodine (purple).

Closed-form **1b** is highly planar except for the two methyl groups which protrude from the molecular plane. The root-mean-square deviation (RMSD) of all non-H atoms from the mean plane (excluding the methyl carbons) is 0.146 Å. The distance of 1.515 Å between C17 and C19 confirms that the diarylethene molecule is the ring-closed isomer.

Molecules of **1b** form 2-D sheets parallel to (010) in which the molecular planes are also parallel to (010). Two crystallographically unique short oxygen-iodine contacts indicate the presence of halogen bonding interactions responsible for the sheet structure with intermolecular I···O distances ($d_{I\cdots O}$) of 2.924 Å and 3.338 Å and corresponding C-I···O angles ($\angle_{C\text{-}I\cdots O}$) of 171.704° and 163.007°, respectively. The sum of the van der Waals radii for oxygen and iodine is 3.50 Å.[57]

The 2-D sheets stack along (010) in repeating and staggered ABAB layers in which a B layer is rotated by 180° around [010]. The layers are staggered such that the protruding methyl groups of two similar sheets (e.g. AA) are directed towards the void of a B layer (Figure 3).

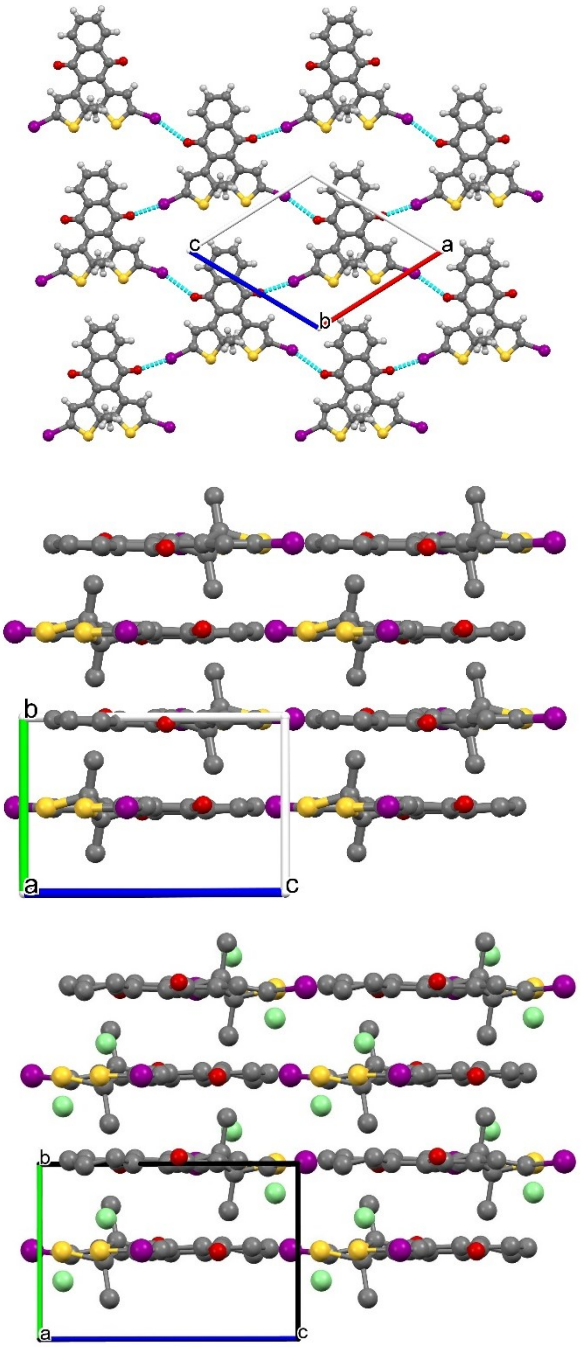


**Figure 3.** Crystal packing diagrams of **1b** viewed down [010] (top) and down [100] (middle) and **1b-irradiated** viewed down [100] (bottom, disordered sulfur atoms colored green). Blue dashed lines indicate halogen bonding interactions.

Viewed under a microscope, single crystals of **1b** appear very dark purple/black and are essentially opaque. Given the strong absorbance, attempts to measure the visible absorption spectrum of a single crystal of **1b** were unsuccessful. Instead, approximately 20 single crystals were gently ground between quartz plates to produce a microcrystalline film (thickness 5.5 µm). The absorption spectrum of the microcrystalline film of **1b** features a maximum at approximately 350 nm and broad absorbance similar to that in solution (Figure S4).

**Electronic Structure**

DFT methods were used to determine the geometry optimized structures and electronic transitions for **1a** and **1b**. Calculations were also performed on a halogen bonded dimer (**XB-dimer**) derived from the crystal structure to assess the impact of the halogen bonding interaction on the spectroscopic properties.

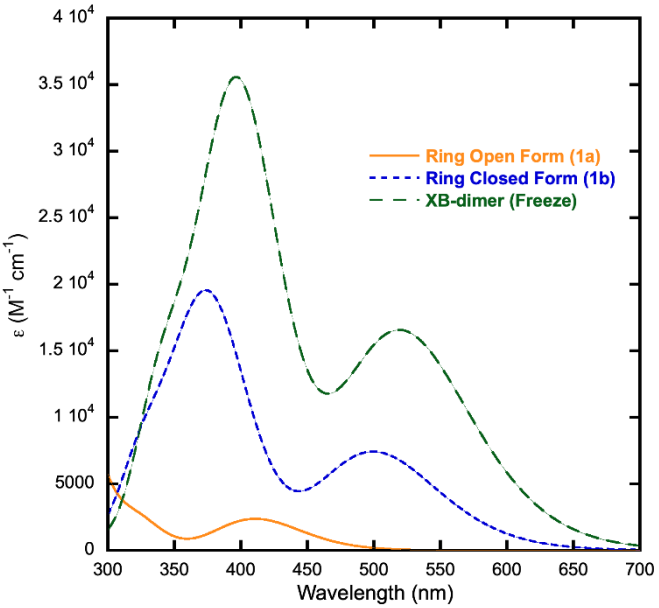


**Figure 4.** Calculated UV-Vis spectra for **1a**, **1b**, and the XB-dimer.

Above 400 nm, **1a** exhibits two strong electronic transitions at 405.81 nm (f=0.0302) and 427.55 nm (f=0.0155) as shown in Figure 4. The maxima at 410 nm in the calculated spectrum is blue shifted by approximately 24 nm relative to **1a** in solution. The largest orbital contributions for the 405 nm and 427 nm transitions are HOMO to LUMO (40.7% and 50.5%) and HOMO-8 to LUMO (27.3% and 30.7%), respectively. The HOMO to LUMO transition may be described as a dithienylethene to napathaquinone transition, whereas the HOMO-8 to LUMO is largely a napthoquinone-based $\pi$ to $\pi^*$ transition (Figure 5).

Isomer **1b** exhibits two strong electronic transitions at 382.28 nm (f=0.2685) and 500.02 nm ((f=0.1413) with two additional weaker transitions at 360.91 nm and 327.7 nm (Figure 4). It should be noted that the stronger calculated oscillator strengths of **1b** relative to **1a** are consistent with the larger extinction coefficients measured for **1b** relative to **1a** (Figure S1). The orbital contribution of the transition at 500 nm is 97.2% HOMO to LUMO whereas the contribution of the 382.27 nm transition is 88.1% HOMO to LUMO+1. The HOMO of **1b** consists largely of π orbitals residing on the dithienylethene and quinone portion of the molecule (Figure 6). The LUMO and LUMO+1 consist of π* orbitals spanning the entire molecule. Thus, both the 382 nm and 500 nm excitations may be described as $\pi$ to $\pi^*$ transitions.

Calculations were also performed on a halogen bonded dimer (**XB-dimer**) using the geometry observed in the crystal structure to assess the impact of this interaction upon the electronic properties of the molecule. The calculated orbitals and contributions for the transitions of **XB-dimer** are very similar to those of **1b** (Tables S1 and S2). The two lowest energy and strongest transitions were calculated to be 400.77 nm (f=0.472) and 520.66 nm ((f=0.3058), a red shift of approximately 20 nm relative to the **1b** monomer. The molecular orbitals of **XB-dimer** associated with the strongest electronic transitions are similar to those for the analogous transitions in **1b** (Figure S5). Likewise, the spectrum of **XB-dimer** strongly resembles that of **1b**, although the maxima are red-shifted. Thus, the presence of halogen bonding interactions is likely responsible for the observed low energy visible absorption.

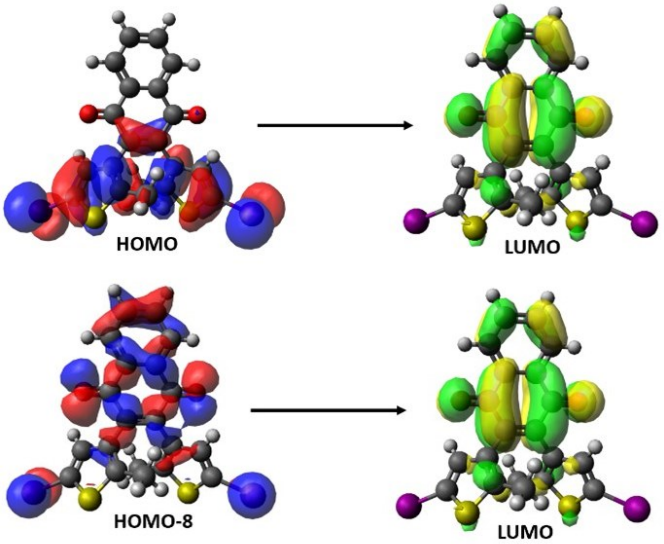


**Figure 5.** Images illustrating the molecular orbitals associated with the HOMO to LUMO transition (top) and the HOMO-8 to LUMO transition (bottom) in **1a**.

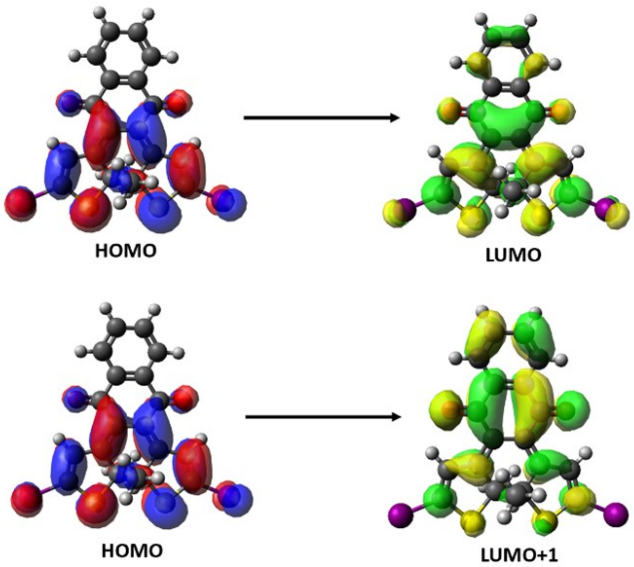


**Figure 6.** Images illustrating the molecular orbitals associated with the HOMO to LUMO transition (top) and HOMO to LUMO+1 transition (bottom) in **1b**.

#### Photocrystallography

Upon irradiation with visible light, crystals of **1b** exhibit the formation of striations approximately parallel to [010] as shown in Figure 7. With continued exposure, the striations separate thus transforming the original single crystal into a collection of smaller crystal fragments described as thin plates or needles. Although these fragments are extremely fragile, one thin plate was mechanically separated, isolated, and analysed by XRD.

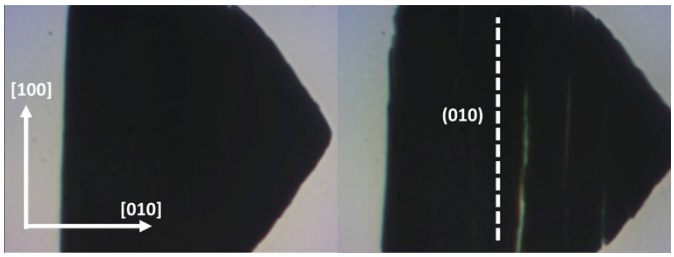


**Figure 7**. Images of a single crystal of 1b viewed normal to (001) before (left) and after (right) irradiation with visible light. Photoinduced cleavage along (010) is indicated with a dashed white line.

Initial refinement of the structure resembled **1b**; however, several q-peaks corresponding to regions of unassigned electron density were observed near the sulphur atoms of the thiophenes. The positions of these q-peaks were consistent with the positions of sulphur atoms of the ring-open isomer, **1a**, that would be formed because of the irradiation**.** The structure was refined using a sulphur disorder model to assess the relative fractions of **1b** and **1a** within the lattice. The resulting occupancies calculated from this model indicated that the lattice contained approximately 7.5(9)% ring-open isomer (**1a**). Examination of the crystal structure of **1b** reveals that the cleavage is consistent with separation of halogen-bonded planes. At the molecular level the separation is likely driven by the strain induced from the formation of the ring-open isomer. Upon ring opening the methyl groups exert a force upon a neighbouring layer which is consistent with the displacement of the disordered sulfur atoms away from the molecular plane (Figure 3). That (010) serves as a photoinduced cleavage plane is likely a consequence of the relatively weak van der Waals interactions between neighbouring (010) sheets when compared to the intermolecular halogen-bonding interactions found within these layers (Figure 5).

## Conclusions

The ability to produce photoactive crystalline materials using ring-closed isomers is an important advance for diarylethene-based crystal engineering. The use of ring-closed isomers effectively eliminates the conformational flexibility present in ring-open isomers that can lead to crystals that contain exclusively photoinactive geometries. This work demonstrates that chemical methods, as opposed to light irradiation, are suitable for producing quantities of ring-closed quinone-based diarylethenes for subsequent crystallization. Future work will assess the potential advantages of chemical ring-closing, namely the suppression of fatigue products that are generated during prolonged irradiation.

The crystal structures confirm that the iodine functional groups of **1b** form intermolecular halogen bonds with oxygen atoms of the quinone moiety. While crystals of **1b** degrade upon exposure to visible light via cleavage planes parallel to the 2-D sheets, this observation confirms that the molecules within the lattice are photoactive and potentially capable of transforming light into mechanical work.

## Conflicts of interest

The authors have no conflicts to declare.

## Author Contributions

SDM, ZYM, JBB and DGP were responsible for conceptualization. SDM, ZYM, TBM, JAS, and DGP were responsible for the investigation. SDM, ZYM, TBM, DGP, and JBB were responsible for the formal analysis. JBB and DGP were responsible for funding acquisition. All authors participated in writing, reviewing, and editing.

## Acknowledgements

Funding was provided by the National Science Foundation, Directorate for Mathematical and Physical Sciences (award No. DMR-2003932) and a Research Development Grant from the Pennsylvania State University at Hazleton.

## Notes and references

1. J. C. Crano and R. J. Guglielmetti, eds., *Organic Photochromic and Thermochromic Compounds*, Plenum Press, New York, 1999.
2. M. Irie, *Chem. Rev.*, 2000, **100**, 1685-1716.
3. M. Herder, B. M. Schmidt, L. Grubert, M. Pätzel, J. Schwarz and S. Hecht, *J. Am. Chem. Soc.*, 2015, **137**, 2738-2747.
4. G. Pariani, M. Quintavalla, L. Colella, L. Oggioni, R. Castagna, F. Ortica, C. Bertarelli and A. Bianco, *J. Phys. Chem. C*, 2017, **121**, 23592-23598.
5. M. Irie, T. Fukaminato, K. Matsuda and S. Kobatake, *Chem. Rev.*, 2014, **114**, 12174-12277.
6. Y.-Y. Tang, Y.-L. Zeng and R.-G. Xiong, *J. Am. Chem. Soc.*, 2022, **144**, 8633-8640.
7. J. Zhang, Q. Zou and H. Tian, *Adv. Mater.*, 2013, **25**, 378-399.
8. R. Wang, L. Diao, Q. Ren, G. Liu and S. Pu, *ACS Omega*, 2019, **4**, 309-319.
9. Y. Zou, T. Yi, S. Xiao, F. Li, C. Li, X. Gao, J. Wu, M. Yu and C. Huang, *J. Am. Chem. Soc.*, 2008, **130**, 15750-15751.
10. V. Lemieux and N. R. Branda, *Org. Lett.*, 2005, **7**, 2969-2972.
11. U. Al-Atar, R. Fernandes, B. Johnsen, D. Baillie and N. R. Branda, *J. Am. Chem. Soc.*, 2009, **131**, 15966-15967.
12. N. A. Simeth, A. C. Kneuttinger, R. Sterner and B. König, *Chem. Sci.*, 2017, **8**, 6474-6483.
13. B. M. Neilson and C. W. Bielawski, *Organometallics*, 2013, **32**, 3121-3128.
14. F. Eisenreich, M. Kathan, A. Dallmann, S. P. Ihrig, T. Schwaar, B. M. Schmidt and S. Hecht, *Nat. Catal.*, 2018, **1**, 516-522.
15. T. Fukaminato, T. Hirose, T. Doi, M. Hazama, K. Matsuda and M. Irie, *J. Am. Chem. Soc.*, 2014, **136**, 17145-17154.
16. T. Sumi, T. Kaburagi, M. Morimoto, K. Une, H. Sotome, S. Ito, H. Miyasaka and M. Irie, *Org. Lett.*, 2015, **17**, 4802-4805.
17. J. Xu, H. Volfova, R. J. Mulder, L. Goerigk, G. Bryant, E. Riedle and C. Ritchie, *J. Am. Chem. Soc.*, 2018, **140**, 10482-10487.
18. X. Deng and L. S. Liebeskind, *J. Am. Chem. Soc.*, 2001, **123**, 7703-7704.
19. D. G. Patel, M. Boggio-Pasqua, T. B. Mitchell, I. M. Walton, W. R. Quigley and F. A. Novak, *Molecules*, 2020, **25**, 2630.
20. D. G. Patel, T. B. Mitchell, S. D. Myers, D. A. Carter and F. A. Novak, *J. Org. Chem.*, 2020, **85**, 2646-2653.
21. M. Quan, D. Sanchez, M. F. Wasylkiw and D. K. Smith, *J. Am. Chem. Soc.*, 2007, **129**, 12847-12856.
22. L. F. Fieser and M. Fieser, *J. Am. Chem. Soc.*, 1935, **57**, 491-494.
23. Y. Kumagai, Y. Shinkai, T. Miura and A. K. Cho, *Annu. Rev. Pharmacool. Toxicol.*, 2012, **52**, 221-247.
24. N. El-Najjar, H. Gali-Muhtasib, R. A. Ketola, P. Vuorela, A. Urtti and H. Vuorela, *Phytochem. Rev.*, 2011, **10**, 353-370.
25. H.-Y. Qiu, P.-F. Wang, H.-Y. Lin, C.-Y. Tang, H.-L. Zhu and Y.-H. Yang, *Chem. Biol. Drug Des.*, 2018, **91**, 681-690.
26. M. Walko and B. L. Feringa, *Chem. Commun.*, 2007, DOI: 10.1039/B702264F, 1745-1747.
27. I. M. Walton, J. M. Cox, C. A. Benson, D. G. Patel, Y.-S. Chen and J. B. Benedict, *New J. Chem.*, 2016, **40**, 101-106.
28. J. M. Cox, I. M. Walton and J. B. Benedict, *J. Mater. Chem. C*, 2016, **4**, 4028-4033.
29. M. Irie, *Photochem. Photobiol. Sci.*, 2010, **9**, 1535-1542.
30. G. R. Desiraju, *J. Am. Chem. Soc.*, 2013, **135**, 9952-9967.
31. C. A. Gunawardana and C. B. Aakeröy, *Chem. Commun.*, 2018, **54**, 14047-14060.
32. S. Cherukuvada, R. Kaur and T. N. Guru Row, *CrystEngComm*, 2016, **18**, 8528-8555.
33. G. R. Desiraju, *Angew. Chem. Int. Ed.*, 1995, **34**, 2311-2327.
34. E. Saito, T. Ako, Y. Kobori and A. Tsuda, *RSC Advances*, 2017, **7**, 2403-2406.
35. S. Kobatake, T. Yamada, K. Uchida, N. Kato and M. Irie, *J. Am. Chem. Soc.*, 1999, **121**, 2380-2386.
36. S. Yamamoto, K. Matsuda and M. Irie, *Chem. Eur. J.*, 2003, **9**, 4878-4886.
37. G. Liu, M. Liu, S. Pu, C. Fan and S. Cui, *Dyes and Pigments*, 2012, **95**, 553-562.
38. G. Cavallo, P. Metrangolo, R. Milani, T. Pilati, A. Priimagi, G. Resnati and G. Terraneo, *Chem. Rev.*, 2016, **116**, 2478-2601.
39. L. C. Gilday, S. W. Robinson, T. A. Barendt, M. J. Langton, B. R. Mullaney and P. D. Beer, *Chem. Rev.*, 2015, **115**, 7118-7195.
40. A. Mukherjee, S. Tothadi and G. R. Desiraju, *Acc. Chem. Res.*, 2014, **47**, 2514-2524.
41. V. Nemec, K. Lisac, N. Bedeković, L. Fotović, V. Stilinović and D. Cinčić, *CrystEngComm*, 2021, **23**, 3063-3083.
42. T. Ichikawa, M. Morimoto and M. Irie, *Photochem. Photobiol. Sci.*, 2014, **13**, 199-204.
43. T. Fukushima, K. Tamaki, A. Isobe, T. Hirose, N. Shimizu, H. Takagi, R. Haruki, S.-i. Adachi, M. J. Hollamby and S. Yagai, *J. Am. Chem. Soc.*, 2021, **143**, 5845-5854.
44. F. Luo, C. B. Fan, M. B. Luo, X. L. Wu, Y. Zhu, S. Z. Pu, W.-Y. Xu and G.-C. Guo, *Angew. Chem. Int. Ed.*, 2014, **53**, 9298-9301.
45. V. I. Nikolayenko, S. A. Herbert and L. J. Barbour, *Chem. Commun.*, 2017, **53**, 11142-11145.
46. D. G. Patel, I. M. Walton, J. M. Cox, C. J. Gleason, D. R. Butzer and J. B. Benedict, *Chem. Commun.*, 2014, **50**, 2653-2656.
47. I. M. Walton, J. M. Cox, T. B. Mitchell, N. P. Bizier and J. B. Benedict, *CrystEngComm*, 2016, **18**, 7972-7977.
48. A. M. Rice, C. R. Martin, V. A. Galitskiy, A. A. Berseneva, G. A. Leith and N. B. Shustova, *Chem. Rev.*, 2020, **120**, 8790-8813.
49. Gaussian 09, Revision D.01, Wallingford, CT, 2009.
50. N. Mardirossian and M. Head-Gordon, *J. Chem. Theory Comput.*, 2016, **12**, 4303-4325.
51. *SMART and SAINTPLUS - Area Detector Control and Integration Software, version 6.01*, Bruker AXS, Madison, WI, 1999.
52. XPREP version 2014/2, Bruker AXS Inc, Madison, Wisconsin, USA, 2014.
53. O. V. Dolomanov, L. J. Bourhis, R. J. Gildea, J. A. K. Howard and H. Puschmann, *J. Appl. Crystallogr.*, 2009, **42**, 339-341.
54. G. Sheldrick, *Acta Crystallogr A*, 2015, **71**, 3-8.
55. G. M. Sheldrick, *Acta Crystallogr. Sect. C: Cryst. Struct. Commun.*, 2015, **71**, 3-8.
56. G. J. P. Perry, J. M. Quibell, A. Panigrahi and I. Larrosa, *J. Am. Chem. Soc.*, 2017, **139**, 11527-11536.
57. A. Bondi, *J. Phys. Chem.*, 1964, **68**, 441-451.